Efficiency Improvement of Universal Motors used in Domestic Appliances

Antonino Di Gerlando, Roberto Perini

Dipartimento di Elettrotecnica - Politecnico di Milano
Piazza Leonardo da Vinci, 32 - 20133 Milano, Italy; phone: +39 - 02 23993722; fax: +39 - 02 23993703
e-mail: [antonino.digerlando; roberto.perini]@ polimi.it

Abstract—**A criterion to improve the efficiency of universal motors used in vacuum cleaners is presented; the lamination external sizes and the stack length are maintained unvaried.**
A mathematical model of the motor is derived, that provides the expressions of torque, current THD, Joule and core losses as a function of the magneto-motive forces and the pole flux. The model is validated by tests and the energy and cost savings related to winding data changing are evaluated. Then, a new lamination internal geometry is studied, that de-saturates rotor teeth, yokes and pole tips, thus increasing the performances.

I. Introduction

Universal motors (UM) are widely adopted in a number of domestic appliances, produced in several millions/year. Typical examples, considered in the following, are UMs for high speed vacuum cleaners, with rated input power of 1.0 ÷ 1.5 kW and rated speed around 30,000 ÷ 45,000 rpm.

The purpose of the paper is to analyse some reduced cost redesign criteria for the performance improvement of the UM – vacuum cleaner system, maintaining unvaried the external motor sizes: this constraint allows to avoid expensive changes of the vacuum cleaner frame geometry.

The work is subdivided as follows:

- a design oriented model is carried out: it allows to express the equivalent circuit parameters and some operating quantities (torque, Joule losses, current THD) as a function of the main electromagnetic variables;
- a low cost redesign criterion of the motor is analysed, just considering the change of the winding data, with totally unvaried motor core geometry (fig.1 left);
- a medium cost, asymmetrical core geometry is studied, with the same external sizes, air-gap profile and stack length, but modified pole tips, yokes and teeth (fig.1 right); it is suited just for motors rotating in one direction.

The flux density maps of the basic motor and of the new one are reported in fig. 1; the new asymmetrical lamination geometry implies the core de-saturation, mainly the pole tips, the stator yoke and the rotor teeth.
For all these cases, the efficiency increase and the reduction of the current distortion are evaluated.

II. Universal Motor Design Modelling

In [1], [2] a basic model of the universal motor has been presented. Here an extension of that model is developed, taking into account the ratio between the stator and rotor turns and the total copper section in the slot. Moreover, all the quantities are given as a function of the magneto-motive forces (m.m.f.s) and of the pole flux φ.
Fig.1 shows the structure of the studied UM, commercially available (data in Table I), and its asymmetrical version.
The motor equivalent circuit and the magnetization characteristics are shown in figures 2, 3 [1-3].

Table I – Main data of the UM under consideration

rated voltage, frequency: V_n [Vrms]; f_n [Hz]	220 ; 50
rated input power: $P_{in\,n}$ [W]	1250
rated speed: Ω_n [r/min]	32,000
Pole shoe half extension ξ_e: brush shifting α	60°; 22.5°
Brush sizes: $b \cdot w \cdot h$ [mm]	6.3 · 10.95 · 37
air gap width δ [mm]	1.47
Rotor diameter D [mm]; axial length ℓ [mm]	38.25 ; 32

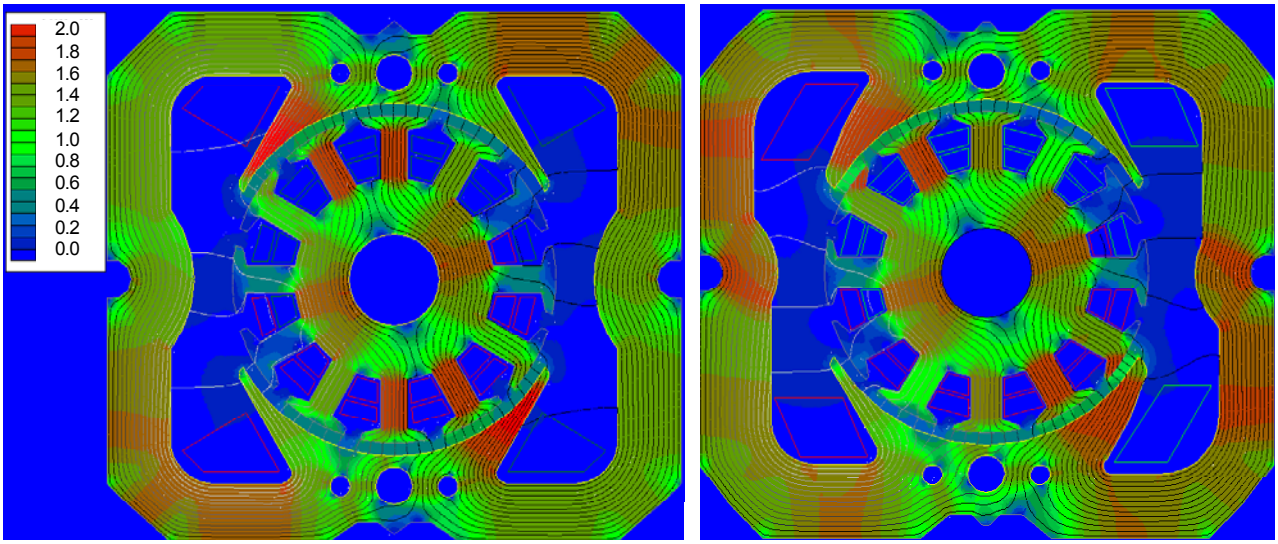

Figure 1. Flux density map of the basic motor symmetrical lamination and of the new asymmetrical lamination (scale in [T]).

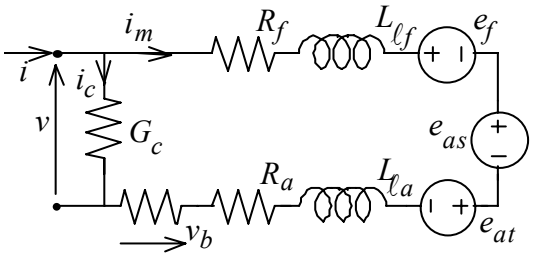

Figure 2. UM equivalent circuit; *Rf*, *Lℓf*, *Ra*, *Lℓa*: field (f) and armature (a) resistance and leakage inductance; *ef*: field e.m.f. induced by the pole flux φ; *eas*, *eat*: speed, transformer armature e.m.f.; *vb*: brush voltage drop; *Gc*: core losses conductance [3].

The armature m.m.f. has a direct and demagnetising component, because of the brush shifting α [1]. Thus, the magnetizing m.m.f. $m_m(t)$ is given by:

$$m_m = (1-\sigma\cdot\alpha)\cdot m_f = (1-\sigma\cdot\alpha)\cdot N_f\cdot i_m \qquad (1)$$

where: $\sigma = (N_a/N_f)/(2\cdot\pi)$ (2)

is the reaction factor, N_a and N_f the number of turns of the armature and field windings (N_f is the number of turns of each pole); $m_f = N_f\cdot i_m$ is the field m.m.f. of each pole.

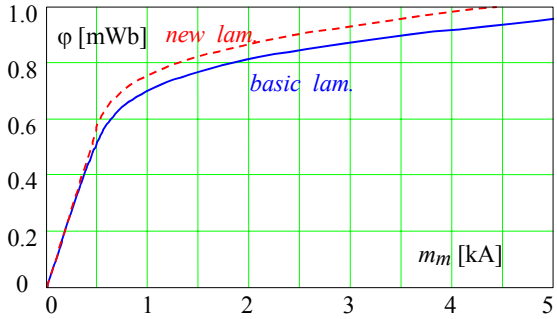

Figure 3. Magnetization characteristics of the basic lamination and of the new asymmetrical lamination (for σ = 0.445; α=22.5°).

As clear from (1), the armature demagnetizing effect depends on the product α·σ; on the other hand, changing the reaction factor σ, a suited new value of the brush shifting α should be adopted, in such a way to obtain acceptable commutation conditions (brush axis coincident with the neutral operating axis).

Thanks to selected FEM analyses, the optimal law $\alpha_o(\sigma)$ has been obtained, as shown in fig.4: experimental tests have confirmed the soundness of the law $\alpha_o(\sigma)$.

In the following, some adopted assumptions are given:

- the operation occurs under sinusoidal voltage feeding;
- an optimal brush shifting law $\alpha_o(\sigma)$ is always adopted;

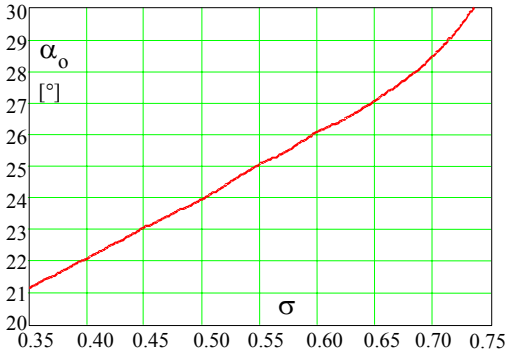

Figure 4. Optimal brush angular position α_o as a function of the reaction factor σ: the best commutation conditions are guaranteed (brush axis coincident with the neutral operating axis).

- the φ(*t*) waveform is practically sinusoidal (as verified both numerically and by tests), with Φ peak pole flux:

$$\varphi(t) = \Phi\cdot\sin(\omega\cdot t)\ ; \qquad (3)$$

- the operation is acceptable if, at the pole tips, the flux density distribution does not show a local inversion.

In terms of instantaneous values, the magnetization characteristics of fig. 3 can be analytically expressed as:

$$m_m(t) = \left(\theta_\delta + \theta_f(\varphi(t))\right)\cdot\varphi = \theta_\delta\cdot\left(1+\rho_\theta(\varphi(t))\right)\cdot\varphi(t) \qquad (4)$$

with θ_δ, $\theta_f(\varphi)$ air-gap and core reluctances respectively.

Thus, the e.m.f.s represented in fig. 2 are given by:

$$e_f = 2\cdot N_f\cdot(d\varphi/dt) = 2\cdot N_f\cdot\omega\cdot\Phi\cdot\cos(\omega\cdot t) \qquad (5)$$

$$e_{at} = C_{at}\cdot N_a\cdot(d\varphi/dt) = C_{at}\cdot N_a\cdot\omega\cdot\Phi\cdot\cos(\omega\cdot t) \qquad (6)$$

$$e_{as} = C_{as}\cdot N_a\cdot\Omega\cdot\varphi = C_{as}\cdot N_a\cdot\Omega\cdot\Phi\cdot\sin(\omega\cdot t) \qquad (7)$$

where:

C_{at} and C_{as} are the transformer and speed linkage coefficients [1], and Ω the angular speed.

The expression of the instantaneous torque can be obtained as follows by the armature speed e.m.f. e_{as}:

$$T(t) = \frac{e_{as}\cdot i_m}{\Omega} = \frac{C_{as}\cdot N_a\cdot\varphi(t)\cdot m_m(t)}{N_f\cdot(1-\sigma\cdot\alpha_o)} = \\ = 2\cdot\pi\cdot C_{as}\cdot\frac{\sigma}{1-\sigma\cdot\alpha_o}\cdot\theta_\delta\cdot\left(1+\rho_\theta(\varphi(t))\right)\varphi(t)^2 \qquad (8)$$

Thus, by integrating eq. (8), the average torque is:

$$T_{av} = \frac{1}{\pi}\cdot\int_0^\pi T(x)\,dx = \frac{C_{as}\cdot\pi\cdot\sigma}{1-\sigma\cdot\alpha_o}\cdot\theta_\delta\cdot\left(1+\rho_{\theta 1}(\Phi)\right)\cdot\Phi^2 \qquad (9)$$

where

$$\rho_{\theta 1}(\Phi) = \frac{2}{\pi}\cdot\int_0^\pi \rho_\theta(\Phi\cdot\sin(\xi))\cdot\sin^2(\xi)\,d\xi \qquad (10)$$

can be called basic average saturation function.

As for the Joule losses (see fig. 2):

$$p_{pJ}(t) = (R_f+R_a)\cdot i_m^2(t) = \frac{(R_f+R_a)\cdot m_m^2(t)}{N_f^2\cdot(1-\sigma\cdot\alpha_o)^2}, \qquad (11)$$

its average value equals:

$$P_{pJ} = \frac{1}{T}\cdot\int_0^T p_{pJ}(t)\,dt = \frac{(R_f+R_a)}{N_f^2\cdot(1-\sigma\cdot\alpha_o)^2}\cdot M_m^2\ , \qquad (12)$$

where M_m is the rms value of the magnetizing m.m.f. $m_m(t)$. Considering eq. (4), it follows:

$$M_m^2 = \frac{1}{\pi}\cdot\int_0^\pi\left(1+\rho_\theta(\varphi)\right)^2\cdot\theta_\delta^2\cdot\varphi^2(x)\cdot dx = \theta_\delta^2\cdot\Phi^2\cdot\frac{1}{\pi}\cdot \\ \cdot\int_0^\pi\sin^2(x)\cdot\left(1+2\cdot\rho_\theta(\Phi\cdot\sin(x))+\rho_\theta^2(\Phi\cdot\sin(x))\right)dx = \\ = \left(\Phi/\sqrt{2}\right)^2\cdot\theta_\delta^2\cdot\left(1+2\cdot\rho_{\theta 1}(\Phi)+2\cdot\rho_{\theta 2}(\Phi)\right) \qquad (13)$$

where

$$\rho_{\theta 2}(\Phi) = \frac{1}{\pi}\cdot\int_0^\pi\sin^2(x)\cdot\rho_\theta{}^2(\Phi\cdot\sin(x))\cdot dx \qquad (14)$$

can be called quadratic average saturation function.

Fig.5 shows the integral saturation functions $\rho_{\theta 1}(\Phi)$ and $\rho_{\theta 2}(\Phi)$ of the basic motor lamination, as a function of the peak pole flux Φ: as observed, around the rated flux (roughly 0.7 mWb), the effect of saturation is relevant.

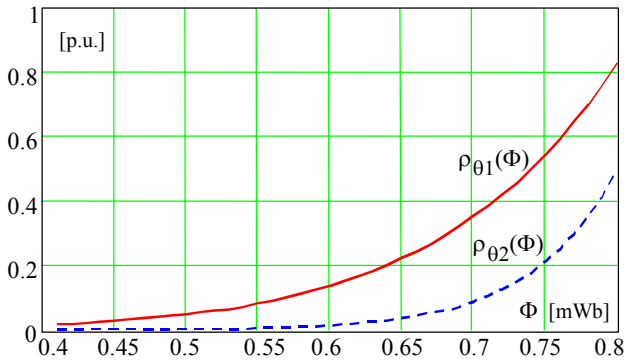

Figure 5. Saturation functions, $\rho_{\theta 1}(\Phi)$, $\rho_{\theta 2}(\Phi)$ (basic motor).

From eq.s (12) and (2), it follows:

$$\frac{\left(R_f+R_a\right)}{N_f^2}=\frac{R_f}{N_f^2}+\frac{R_a}{N_a^2}\cdot\frac{N_a^2}{N_f^2}=R_{f1}+R_{a1}\cdot\left(2\cdot\pi\cdot\sigma\right)^2, \quad (15)$$

with R_{f1} and R_{a1} field and armature "one turn" winding resistances, evaluated with the actual turn average length and with the total copper cross section of the considered windings (in the following assumed invariable).
Thus, the average Joule losses become:

$$P_{pJ}=\frac{R_{f1}+R_{a1}\cdot\left(2\cdot\pi\cdot\sigma\right)^2}{2\left(1-\sigma\cdot\alpha_o\right)^2}\cdot\theta_\delta^2\cdot\Phi^2\cdot \cdot\left(1+2\cdot\left(\rho_{\theta 1}(\Phi)+\rho_{\theta 2}(\Phi)\right)\right) \quad (16)$$

The brush losses $p_{pb} = v_b(i)\cdot i$ are due to the voltage drops in the brush body and at the brush-commutator contact:

$$v_b\approx R_{bb}\cdot i_r\cdot\left(i/i_r\right)+V_{cb}\cdot\left(i/i_r\right)^{\kappa_b}\approx \approx V_{bbr}\cdot\left(m_m/m_{mr}\right)+V_{cbr}\cdot\left(m_m/m_{mr}\right)^{\kappa_b} \quad (17)$$

(reference values for the motor of fig.1 are (subscript *r*): $V_{bbr}\approx 6$ V; $V_{cbr}\approx 3$ V; $\kappa_b\approx 0.52$; $P_{pbr}\approx 52$ W) .
Concerning the core losses P_{pc}, whose most important contribution is given by the rotor losses at the internal frequency f_i, they can be estimated as follows [3]:

$$P_{pc}=P_{pcr}\cdot\left(\Phi/\Phi_r\right)^2\cdot\left(f_i/f_{ir}\right)^{n_c} \quad (18)$$

(in the motor of fig.1, the reference values are: f_{ir}= 650 Hz, Φ_r = 0.7 mWb: P_{pcr}= 52 W; n_c= 1.82).
As for the voltage equation, from fig.2 and eq.s (5)-(7):

$$v(t)=\left(R_f+R_a+R_b\right)\cdot i_m(t)+\left(L_{\ell f}+L_{\ell a}\right)\cdot\left(d\,i_m/d\,t\right)+ +e_f(t)+e_{at}(t)+e_{as}(t) \quad (19)$$

If the applied voltage $v(t)$ is sinusoidal, the flux $\varphi(t)$ and the e.m.f.s $e_f(t)$, $e_{at}(t)$, $e_{as}(t)$ are practically sinusoidal, too. It follows that the quantity:

$$\left(R_f+R_a+R_b\right)\cdot i_m(t)+\left(L_{\ell f}+L_{\ell a}\right)\cdot\left(d\,i_m/d\,t\right)= =R_{eq}\cdot i_m(t)+L_{\ell eq}\cdot\left(d\,i_m/d\,t\right) \quad (20)$$

must vary sinusoidally. Subdividing the magnetizing current into a first harmonic and a residual:

$$i_m(t)=i_{m1}(t)+i_{mres}(t)\ , \quad (21)$$

then:

$$R_{eq}\cdot i_m(t)+L_{\ell eq}\cdot\frac{d\,i_m}{d\,t}=R_{eq}\cdot i_{m1}(t)+L_{\ell eq}\cdot\frac{d\,i_{m1}}{d\,t}\ . \quad (22)$$

From eq.s (22) and (1):

$$R_{eq}\cdot i_{m1}(t)=\frac{R_{eq}\cdot m_{m1}(t)}{N_f\cdot\left(1-\sigma\cdot\alpha_o\right)}=N_f\cdot\frac{R_{eq}}{N_f^2}\cdot\frac{m_{m1}(t)}{\left(1-\sigma\cdot\alpha_o\right)} \quad (23)$$

where, by (15):

$$\frac{R_{eq}}{N_f^2}=\frac{\left(R_b+R_f+R_a\right)}{N_f^2}=\frac{R_b}{N_f^2}+R_{f1}+R_{a1}\cdot\left(2\cdot\pi\cdot\sigma\right)^2 \quad (24)$$

and

$$L_{\ell eq}\cdot\frac{d\,i_{m1}}{d\,t}=\frac{L_{\ell eq}}{N_f\cdot\left(1-\sigma\cdot\alpha_o\right)}\cdot\frac{d\,m_{m1}}{d\,t}= =\frac{N_f^2\cdot\Lambda_{\ell f}+N_a^2\cdot\Lambda_{\ell a}}{N_f\cdot\left(1-\sigma\cdot\alpha_o\right)}\cdot\frac{d\,m_{m1}}{d\,t}= =N_f\cdot\frac{\Lambda_{\ell f}+\left(2\cdot\pi\cdot\sigma\right)^2\cdot\Lambda_{\ell a}}{\left(1-\sigma\cdot\alpha_o\right)}\cdot\frac{d\,m_{m1}}{d\,t} \quad (25)$$

In this way, the applied voltage $v(t)$ gets:

$$v(t)=N_f\cdot\left(\frac{R_{eq}}{N_f^2}\cdot\frac{m_{m1}}{\left(1-\sigma\cdot\alpha_o\right)}+\frac{\Lambda_{\ell f}+\left(2\cdot\pi\cdot\sigma\right)^2\Lambda_{\ell a}}{\left(1-\sigma\cdot\alpha_o\right)}\cdot \cdot\frac{d\,m_{m1}}{d\,t}+2\cdot\left(1+\pi\cdot\sigma\cdot C_{at}\right)\cdot\omega\cdot\Phi\cdot\cos(\omega\cdot t)+ +2\cdot\left(\pi\cdot\sigma\cdot C_{as}\right)\cdot\Omega\cdot\Phi\cdot\sin(\omega\cdot t)\right) \quad (26)$$

The quantities in eq. (26) are sinusoidal; moreover, $m_{m1}(t)$ and $\varphi(t)$ are in phase. Recalling eq.(3) and expressing all the quantities as phasors, it follows:

$$\bar{V}=N_f\cdot\bar{\Phi}\cdot\left(\left(\frac{R_{eq}}{N_f^2}\cdot\frac{\theta_\delta\cdot\left(1+\rho_{\theta 1}(\Phi)\right)}{\left(1-\sigma\cdot\alpha_o\right)}+2\pi\sigma C_{as}\,\Omega\right)+j\,\omega\cdot \cdot\left(\frac{\Lambda_{\ell f}+\left(2\pi\sigma\right)^2\Lambda_{\ell a}}{\left(1-\sigma\cdot\alpha_o\right)}\theta_\delta\left(1+\rho_{\theta 1}(\Phi)\right)+2\left(1+\pi\sigma C_{at}\right)\right)\right) \quad (27)$$

The rms field and armature current densities are:

$$S_f=\frac{I_m}{A_{cf}}=\frac{\theta_\delta\cdot\sqrt{1+2\cdot\rho_{\theta 1}(\Phi)+2\cdot\rho_{\theta 2}(\Phi)}}{A_{cu.f}\cdot\left(1-\sigma\cdot\alpha_o\right)}\cdot\frac{\Phi}{\sqrt{2}} \quad (28)$$

and

$$S_a=\frac{A_{cu.f}}{A_{cu.a}\cdot c_r}\cdot\left(2\cdot\pi\cdot\sigma\right)\cdot S_f \quad (29)$$

where A_{cf}, $A_{cu.f}$ are the cross sections of one field conductor and of all the conductors of the N_f turns of each field pole, respectively; $A_{cu.a}$ is the cross section of all the conductors in one rotor slot; c_r is the N° of rotor slots.
The current distortion factor ν can be evaluated as follows:

$$\nu=\frac{M_{m1}}{M_m}=\frac{\theta_\delta\cdot\left(1+\rho_{\theta 1}(\Phi)\right)\cdot\left(\Phi/\sqrt{2}\right)}{\theta_\delta\cdot\sqrt{1+2\rho_{\theta 1}(\Phi)+2\rho_{\theta 2}(\Phi)}\cdot\left(\Phi/\sqrt{2}\right)}= =\frac{1+\rho_\vartheta(\Phi)}{\sqrt{1+2\rho_{\theta 1}(\Phi)+2\rho_{\theta 2}(\Phi)}} \quad (30)$$

Thus, the THD_I of the current equals:

$$THD_I=\sqrt{\frac{M_m^2}{M_{m1}^2}-1}=\sqrt{\frac{1}{\nu^2}-1}=\ldots=\frac{\sqrt{2\cdot\rho_{\theta 2}-\rho_{\theta 1}^2}}{1+\rho_{\theta 1}} \quad (31)$$

III. Model validation and Low Cost Redesign Strategies of UM for vacuum cleaners

The efficiency improvement of the whole system implies some redesign actions both on the turbine and on the electric motor. As for the former, the diameter should be reduced, increasing the angular speed and modifying the shape of the air baffle. Obviously, in a good design, the maximum turbine efficiency should occur at the most frequent operating speed of the turbine, and should match the maximum motor efficiency. Some typical efficiency curves of the turbine are reported in fig.6: in the following, we will assume that the turbine is not modified.

As for the electric motor, the model, derived from the preceding equations, has been experimentally verified.

Fig.s 7a and 7b show simulated and test results of a motor-turbine basic system (*B*), with no core modifications, operating connected to a standard vacuum box emulating the vacuum cleaner. The box is a cube of 500 mm per side, with two holes: the motor is leaned over the first one, while the diameter D_h of the second (air inlet hole) is varied, emulating different dust sack filling conditions.

The following remarks can be made:

- the model accuracy is fair, as shown by the test-simulation agreement;
- the efficiency of the system is greatly limited by the turbine efficiency; moreover, the maximum efficiency condition occurs in a limited operating range, while the motor efficiency curve shows higher levels and is flatter.

In the following, some motor redesign examples will be analysed, by using the developed model, and the related performance improvements will be evaluated.

A first low-cost redesign criterion (called R_L) maintains unvaried the motor sizing, that is the total copper, iron mass and lamination geometry are constant. It is based on the reduction of the design value of the peak flux Φ, keeping constant the torque value at a chosen reference speed. The positive consequences of this strategy are:

- mitigation of the Joule losses (thanks to the decrease of Φ^2, $\rho_{\theta 1}$ and $\rho_{\theta 2}$, see eq.s (12), (13), (14));
- electrical brush losses reduction (thanks to the current reduction, see eq.s (4), (17));
- core losses decrease (eq. (18)), and reduction of the current distortion (eq. (31));
- better motor efficiency, commutation, thermal conditions.

As declared, the losses reduction should maintain unvaried the torque at a reference speed.

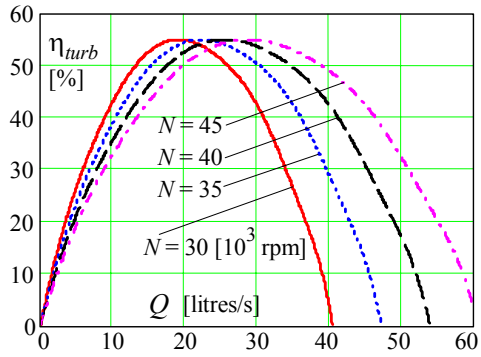

Fig.6 – Aeraulic efficiency curves of the vacuum cleaner turbine, as a function of the air flow, with the angular speed as parameter.

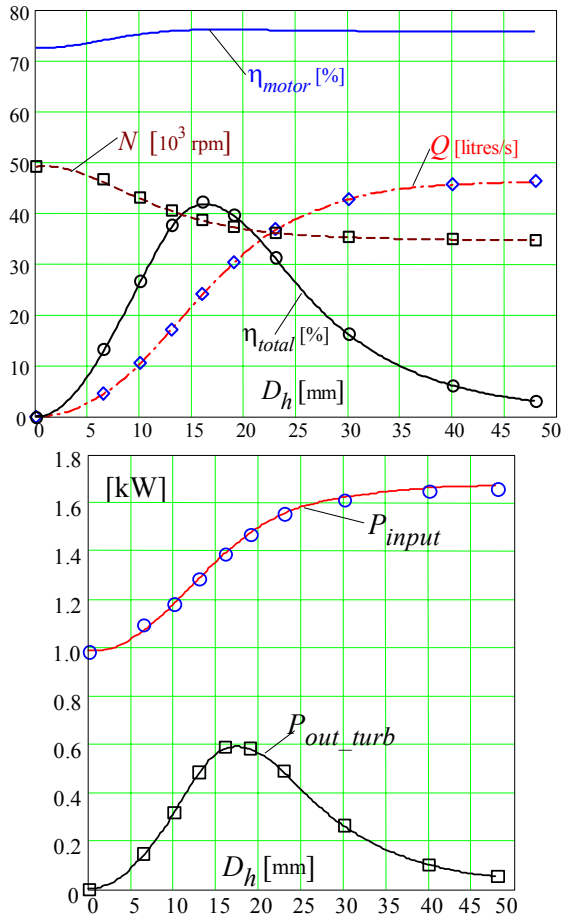

Figures 7a, 7b. Simulated values (continuous lines) and experimental results (points O, ◇ and □) of the basic motor-turbine system (*B*), operating connected to a standard vacuum box emulating various dust sack filling conditions of the vacuum cleaner (by different values of the air inlet hole diameter D_h). Winding data of the basic motor: N° of turns: N_a = 324; N_f = 116; wire diameters: d_a = 0.42 mm; d_f = 0.71 mm.

By observing eq. (9), this goal can be achieved by suitably increasing the reaction factor σ, so as to compensate the flux Φ decrease.

The reference speed can be maintained unvaried by adopting a suitable value of the number of field turns N_f, to be obtained by solving the voltage phasor equation (27).

Of course, the increase of σ is restricted by the need to limit the reaction armature m.m.f., that could excessively distort the air-gap field distribution: as a consequence, the commutation would get worse.

Fig.s 8a and 8b show the results of a motor redesign, according to the criterion R_L: the motor redesign implies a reduction of 15% of the peak flux Φ, maintaining unvaried the system conditions in the operating point characterized by a hole diameter D_h = 16 mm, that is the diameter of maximum total efficiency.

The simulations have shown that the output performances remain exactly unvaried all along the diameter D_h range; as regards the input motor behaviour, fig.s 8a and 8b show the reduction of the current distortion and of the motor losses in the same D_h range.

The observation of the motor loss reduction ΔP_p (corresponding to an equivalent input power reduction) could suggest that the energy saving is poor.

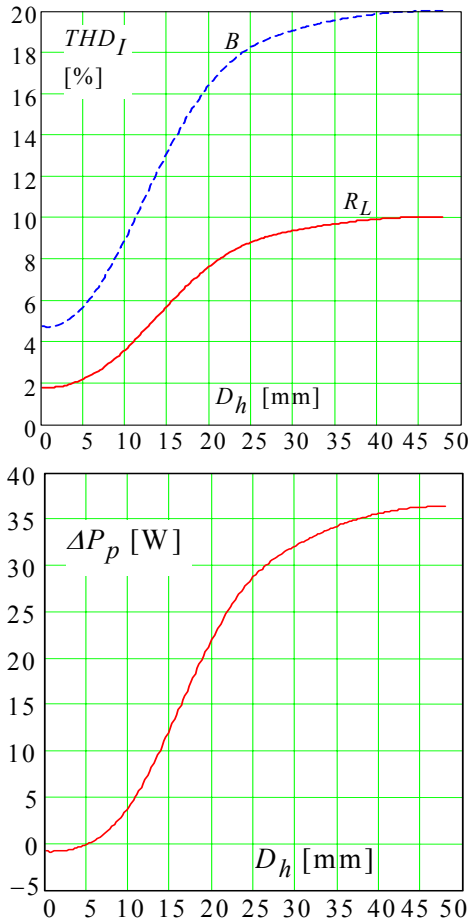

Figures 8a, 8b. Results of the motor redesign according to the criterion R_L (reduction of 15% of the peak flux Φ, maintaining unvaried the output system operation with a hole diameter D_h = 16 mm): reduction of the current THD and of the losses, compared with the corresponding quantities of the basic motor *B*. Winding data of the motor redesigned according R_L: N° of turns: Na = 372; Nf = 98; wire diameters: da = 0.40 mm; df = 0.75 mm.

Some additional remarks can help in evaluating the actual savings: considering that the hole diameter D_h variation emulates all the conditions of the dust sack filling (apart from diameters under a minimum value D_{hm}, for which the air flow is so low that the user is advised to empty the sack), the average loss reduction equals:

$$\Delta P_{p_{av}} = \frac{1}{(D_{hM} - D_{hm})} \int_{D_{hm}}^{D_{hM}} \Delta P_p(D_h) \cdot dD_h \quad . \quad (32)$$

With D_{hm} = 6 mm, D_{hM} = 48 mm, one obtains: $\Delta P_{p_{av}}$ = 25.0 W. With a motor life of Δt_L = 600 h, an energy cost of C_E = 0.13 €/kWh and a production of M_P = $6 \cdot 10^6$ motors/year (production of a leader manufacturer in Italy), Table II shows some results: even if the savings of one final user are limited, the savings during the life of a one-year motor population are interesting.

Table II. Energy and cost savings for one motor and one-year motor production population ($MP = 6 \cdot 10^6$), obtainable from the basic motor *B*, redesigned according to the R_L criterion.

one motor energy saving [kWh]	$\Delta P_{p_{av}} \cdot \Delta t_L$	15.0
one motor cost saving [€]	$C_E \cdot \Delta P_{p_{av}} \cdot \Delta t_L$	1.95
M_P motors energy saving [GWh]	$M_P \cdot \Delta P_{p_{av}} \cdot \Delta t_L$	90.0
M_P motors cost savings [M€]	$M_P \cdot C_E \cdot \Delta P_{p_{av}} \cdot \Delta t_L$	11.7

IV. UM Medium Cost Redesign Strategies with Lamination Changes

In order to limit the cost impact, according to this strategy (called R_M), the core external layout and the stack length are maintained unvaried (due to vacuum cleaner sizes constraints), together with the air-gap geometry. The modifications are finalised to reduce the local saturations caused by the armature reaction: thus, the internal geometry of the magnetic core is modified, adopting an asymmetrical configuration, both on the pole tips and on the stator yoke (fig. 1 right). This leads to compensate the cited asymmetrical saturations, allowing a performance improvement of the motor, without increasing the whole external dimensions. (N.B.: the asymmetrical redesign is possible if the motor rotates only in one direction; the same can be stated out for the brush shifting, here adopted).
The re-distribution of the magnetic flux in the core allows to obtain the following global and local effects:

- an increase of the flux Φ, with unvaried m_m (fig. 3): thus the torque increases, being the motor losses equal;
- a reduction of the local saturation, particularly in the saturated pole tips; the consequence is an improvement of the commutation conditions, thus of the brush life.

The choice of the winding data has been carried out leaving from the basic (*B*) motor, following these steps:

- with a hole diameter of 16 mm, increase of the motor speed, maintaining roughly unvaried the motor losses with respect to the basic motor;
- unvaried brush shifting angle α (α = 22.5°);
- choice of the reaction factor σ (eq. 2) according to the optimal law $\alpha_o(\sigma)$, with α = 22.5° (fig. 4);
- choice of the N° of turns of the field and armature windings, in order to satisfy the voltage equation (26);
- choice of the wire cross sections leaving from equations (28), (29), with current density values roughly unvaried.

The simulation results are presented in the following.
Fig.9 shows the increase of the UM output power, obtainable with the strategy R_M, by adopting the new lamination according to the described criteria.

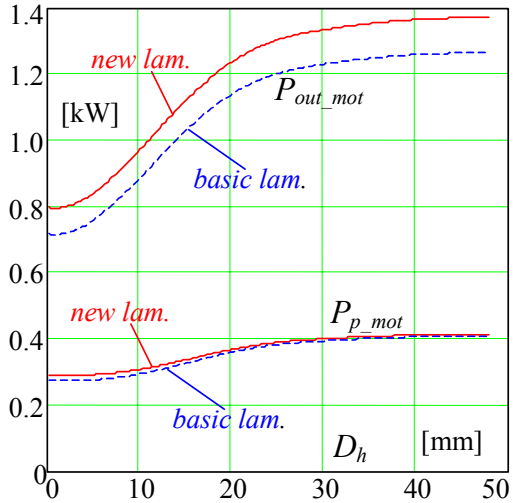

Figure 9. Losses ($P_{p.mot}$) and output power ($P_{out.mot}$) of the UM: dotted curves: basic lamination (fig.1, left) and motor (B); solid curves: new lamination (fig.1, right).
Winding data of the UM redesigned according R_M: N° of turns: Na = 300; Nf = 107; wire diameters: da = 0.45 mm; df = 0.75 mm.

As can be seen, the motor losses are slightly increased: anyway, this fact does not imply thermal problems, thanks to the better cooling due to the speed increase.

Fig.10 shows the motor efficiency improvement, roughly higher by 1%: this positive result impacts also on the global system efficiency, as shown in detail in fig.11, even if in a reduced amount, because of the low turbine efficiency level. Finally, fig.12 shows how the asymmetrical lamination allows to reduce the current distortion, thanks to the lower saturation level.

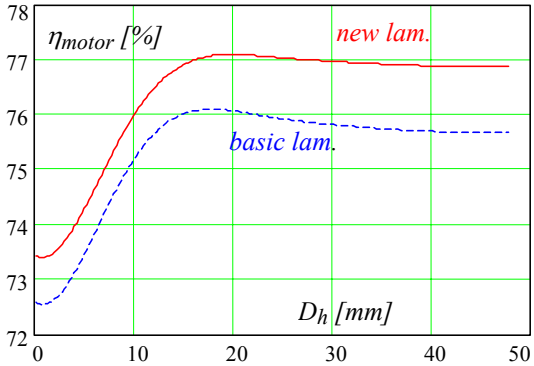

Figure 10. Asymmetrical motor: motor efficiency increase with respect to the efficiency of the motor with the basic lamination.

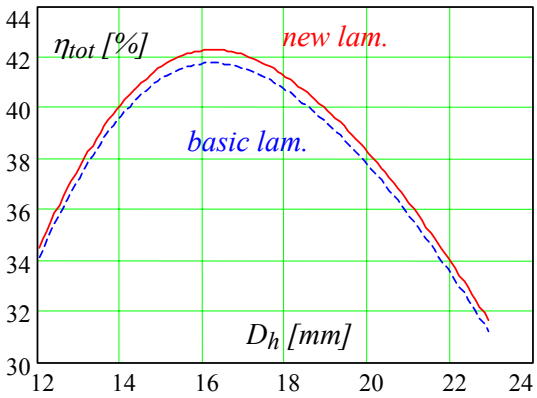

Figure 11. Asymmetrical motor: increase of the total efficiency (motor + turbine) with respect to that of the basic motor system.

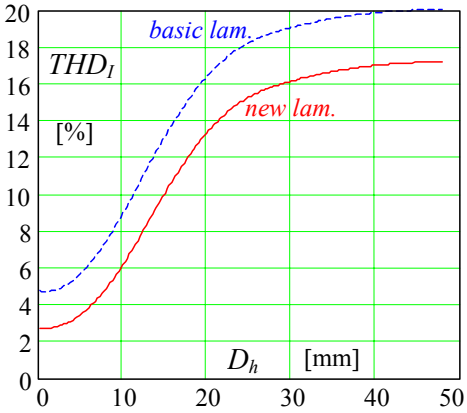

Figure 12. Decrease of the motor current THD_I of the asymmetrical lamination with respect to that of the basic motor.

V. Conclusion

In the paper, a design oriented model of the UM has been derived, suited to obtain the expressions of torque, Joule and core losses, efficiency and current THD as a function of the main magnetic quantities (magneto-motive forces and pole flux).

This model has been validated by tests, showing an excellent agreement with the experimental results.

Subsequently, the model has been adopted for the analysis of two redesign methods, aimed to improve the performances of the universal motors used in vacuum cleaners (efficiency, output power, current distortion).

A first, low cost, criterion has considered the motor losses reduction, being the same the output power, just modifying the winding data and the brush shifting angle.

A second, medium cost, criterion was based on the invariance of the motor losses, increasing the output power, thank to the adoption of an asymmetrical lamination, being the same the stator external sizes.

These criteria have been tested, giving encouraging results, substantially confirming the theoretical results.

Acknowledgement

Work supported by the Italian National Ministry of Education, University and Research (MIUR), Grant Cofin 2001, Title: “Improvement of the energy efficiency of electrical motors and drives for industrial and civil applications”.

References

[1] A. Di Gerlando, R. Perini, G. Rapi: “Equivalent Circuit for the Performance Analysis of UMs”, *IEEE Trans. on Energy Conversion*, Vol.19, N.1, March 2004.

[2] A. Di Gerlando, R. Perini: “A Model for the Operation Analysis of High Speed Universal Motors with Triac Regulated Mains Voltage Supply”; *SPEEDAM 2002, Proceedings of the International Symposium on Power Electronics, Electrical Drives, Automation, Motion*, Ravello, Italy, June 11th –14th, 2002.

[3] A. Di Gerlando, R. Perini: “Modelling and Experimental Analysis of Core Saturation and Losses of Universal Motors”; *ICEM 2002, Proc. of the Intern. Conf. on Electrical Machines*; Brugge, Belgium, 25-28 August 2002; Conf. Record on CD: Paper N° 090.

[4] M. Poloujadoff, D. Roye, "Etude du Fonctionnement des Moteurs Universels de petit Puissance" *RGE* - Tome 86 - n° 9, pp. 633-643, September 1977.

[5] T. Fujii, "Study of Universal Motors with lag Angle Brushes" *IEEE Trans. on Power Apparatus & Systems*, Vol. PAS-101, n° 6, pp.1288-1296, June 1982.

[6] R. Ebben, J. Brauer, Z. Cendes, N. Demerdash, "Prediction of Performance Characteristics of a Universal Motor using parametric Finite Element Analysis" *Intern. Conf. on Electric Machines and Drives, IEMD '99*, pp. 192-194.

[7] T. McDermott, P. Zhou, J. Gilmore, Z. Cendes, "Electromechanical System Simulation with Models generated from FEM Solutions" *IEEE Trans. on Magnetics*, vol. 33, no 2, pp.1682-1685, March 1997.

[8] A. Di Gerlando, R. Perini, L. Madonini: “Brush Wear Modelling in High Speed Universal Motors”, *SPEEDAM 2004,* Capri, Italy, June 16-18, 2004.